OXFORD

JNCI J Natl Cancer Inst (2017) 109(7): djw296

doi: 10.1093/jnci/djw296
First published online March 9, 2017
Article

ARTICLE

Role of YAP1 as a Marker of Sensitivity to Dual AKT and P70S6K Inhibition in Ovarian and Uterine Malignancies

Rebecca A. Previs, Guillermo N. Armaiz-Pena, Cristina Ivan, Heather J. Dalton, Rajesha Rupaimoole, Jean M. Hansen, Yasmin Lyons, Jie Huang, Monika Haemmerle, Michael J. Wagner, Kshipra M. Gharpure, Archana S. Nagaraja, Justyna Filant, Michael H. McGuire, Kyunghee Noh, Piotr L. Dorniak, Sarah L. Linesch, Lingegowda S. Mangala, Sunila Pradeep, Sherry Y. Wu, Anil K. Sood

Affiliations of authors: Department of Gynecologic Oncology and Reproductive Medicine (RAP, HJD, RR, JMH, YL, JH, MH, MJW, KMG, ASN, JF, MHM, KN, PLD, SLL, LSM, SP, SYW, AKS), Department of Cancer Biology (AKS), and Center for RNA Interference and Non-Coding RNAs (CI, LSM, AKS), The University of Texas MD Anderson Cancer Center, Houston, TX; Department of Basic Sciences, Division of Pharmacology, Ponce Health Sciences University, Ponce, Puerto Rico (GNAP); Division of Cancer Biology, Ponce Research Institute, Ponce, Puerto Rico (GNAP)

See the Notes section for the full list of authors and affiliations.
Corresponding Author: Anil K. Sood, MD, Departments of Gynecologic Oncology and Cancer Biology, Unit 1362, The University of Texas MD Anderson Cancer Center, 1515 Holcombe Boulevard, Houston, TX 77230 (e-mail: asood@mdanderson.org).

Abstract

Background: The PI3K/AKT/P70S6K pathway is an attractive therapeutic target in ovarian and uterine malignancies because of its high rate of deregulation and key roles in tumor growth. Here, we examined the biological effects of MSC2363318A, which is a novel inhibitor of AKT1, AKT3, and P70S6K.
Methods: Orthotopic murine models of ovarian and uterine cancer were utilized to study the effect of MSC2363318A on survival and regression. For each cell line, 10 mice were treated in each of the experimental arms tested. Moreover, in vitro experiments in 21 cell lines (MTT, immunoblot analysis, plasmid transfection, reverse phase protein array [RPPA]) were carried out to characterize underlying mechanisms and potential biomarkers of response. All statistical tests were two-sided.
Results: MSC2363318A decreased tumor growth and metastases in multiple murine orthotopic models of ovarian (SKOV3ip1, HeyA8, and Igrov1) and uterine (Hec1a) cancer by reducing proliferation and angiogenesis and increasing cell death. Statistically significant prolonged overall survival was achieved with combination MSC2363318A and paclitaxel in the SKUT2 (endometrioid) uterine cancer mouse model ($P < .001$). Mice treated with combination MSC2363318A and paclitaxel had the longest overall survival (mean = 104.2 days, 95% confidence interval [CI] = 97.0 to 111.4) compared with those treated with vehicle (mean = 61.9 days, 95% CI = 46.3 to 77.5), MSC2363318A alone (mean = 89.7 days, 95% CI = 83.0 to 96.4), and paclitaxel alone (mean = 73.6 days, 95% CI = 53.4 to 93.8). Regression and stabilization of established tumors in the Ishikawa (endometrioid) uterine cancer model was observed in mice treated with combination MSC2363318A and paclitaxel. Synergy between MSC2363318A and paclitaxel was observed in vitro in cell lines that had an IC50 of 5 μM or greater. RPPA results identified YAP1 as a candidate marker to predict cell lines that were most sensitive to MSC2363318A ($R = 0.54$, $P = .02$). After establishment of a murine ovarian cancer model of adaptive anti-angiogenic resistance (SKOV3ip1-luciferase), we demonstrate that resensitization to bevacizumab occurs with the addition of MSC2363318A, resulting in improved overall survival ($P = .01$) using the Kaplan-Meier method. Mice treated with bevacizumab induction followed by MSC2363318A had the longest

Received: April 29, 2016; **Revised:** September 5, 2016; **Accepted:** November 8, 2016

overall survival (mean = 66.0 days, 95% CI = 53.9 to 78.1) compared with mice treated with control (mean = 42.0 days, 95% CI = 31.4 to 52.6) and bevacizumab-sensitive mice (mean = 47.2 days; 95% CI = 37.5 to 56.9).
Conclusions: MSC2363318A has therapeutic efficacy in multiple preclinical models of ovarian and uterine cancer. These findings support clinical development of a dual AKT/P70S6K inhibitor.

The PI3K/AKT/mTOR pathway plays a pivotal role in many malignant features involved in tumor pathogenesis (1). The PIK3CA gene is a commonly mutated oncogene, affecting more than 30% of solid tumors (2). PTEN, which encodes phosphatase and tensin homolog, is frequently mutated or suppressed, leading to activation of the PI3K/AKT signaling pathway (3). Ovarian and uterine cancers exhibit alterations in these pathways (4). Frequent aberrations of this pathway in ovarian cancer include mutations in PTEN (5) or hypermethylation of the promoter (6), loss of heterozygosity at the INPP4B locus (7), somatic mutations in mTOR and AKT1 (8), amplification of AKT2 (9), somatic activating mutations in the PIK3CA gene (10), and activating mutations in the PIK3R1 gene (11). Alterations of the PI3K/AKT signaling pathway in ovarian cancers are histology specific; high-grade serous ovarian cancers frequently exhibit amplifications in PIK3CA and in one of the AKT isoforms in up to 20% and 10% to 15% of cases, respectively. Mutations of PIK3CA occur in up to 20% endometrioid and 35% of clear cell ovarian carcinomas. PTEN loss of function mutations are found in 20% of endometrioid ovarian carcinomas (12). The high prevalence of these molecular alterations in ovarian and uterine cancers represents an important therapeutic opportunity.

Dual AKT/P70S6K inhibition provides a novel therapeutic approach by promoting improved PI3K/AKT pathway inhibition while avoiding the negative effects of AKT activation through compensatory feedback loops, including IRS-1. Additionally, inhibition of two targets further downstream in a hyperactive pathway in solid malignancies could avoid the side effects seen with historical pan-PI3K inhibitors. MSC2363318A (EMD Serono) is a highly kinase-selective, ATP-competitive inhibitor of AKT1, AKT3, and P70S6K (13). Here, we examine the biological effects of MSC2363318A in orthotopic murine models of ovarian and uterine cancer and identify YAP1 as a potential predictor of response.

Methods

For a full description of the following experiments, please see the Supplementary Methods (available online).

Laboratory Measures

All cell lines were maintained in 5% CO2 at 37°C. Ovarian cancer (A2780, ES2, HeyA8, Igrov1, Ovcar3, Ovcar4, Ovcar5, Ovcar8, Ovca432, and SKOV3ip1) and uterine cancer (AN3CA, Hec1A, Hec1B, Hec265, Ishikawa, KLE, RL95-2, Spec2, SKUT2, and KLE) cell lines were obtained from the American Type Culture Collection. The Ishikawa-luciferase and SKOV3-luciferase cell lines were made following stable transduction with lentivirus carrying the luciferase gene (the lentiviral vector was kindly provided by Craig Logsdon's lab at UT MD Anderson Cancer Center).

In Vivo Models

Six- to eight-week-old female athymic nude mice were purchased from Taconic Farms (Hudson, NY). These mice were cared for according to guidelines set forth by the American Association for Accreditation of Laboratory Animal Care and the US Public Health Service policy on Human Care and Use of Laboratory Animals. All mouse studies were approved and supervised by The University of Texas MD Anderson Cancer Center Institutional Animal Care and Use Committee.

Reverse Phase Protein Arrays

Igrov1, Ovcar5, Hec1b, Ishikawa, RL95-2 KLE, RF-24 cells sensitive to bevacizumab and RF-24 cells resistant to bevacizumab were treated with 1 μM MSC2363318A for 18 hours. Cellular proteins were denatured by 1% SDS (with beta-mercaptoethanol) and diluted in five twofold serial dilutions in dilution buffer (lysis buffer containing 1% SDS). Serial diluted lysates were arrayed on nitrocellulose-coated slides (Grace Biolab) by Aushon 2470 Arrayer (Aushon BioSystems). A total of 5808 array spots were arranged on each slide, including the spots corresponding to positive and negative controls prepared from mixed cell lysates or dilution buffer, respectively.

Statistical Analysis

Continuous variables were compared with the two-sample *t* test (between two groups) or with analysis of variance (ANOVA; for all groups) if normally distributed (as determined by the Kolmogrov-Smirnov test). For variables with nonparametric distribution, the Kruskal-Wallis test and Dunn's post-test were used for multiple comparisons. All statistics were calculated by GraphPad Prism. Survival experiments were analyzed by the Kaplan-Meier method. A *P* value of less than .05 from a two-tailed statistical test was considered statistically significant. All statistical tests were two-sided unless otherwise noted. A right tail Fisher exact test used to calculate *P* values where indicated.

Isobologram analyses were performed to calculate a combination index as previously described (38–40).

Results

Therapeutic Efficacy of MSC2363318A in Orthotopic Models of Ovarian and Uterine Cancer

First, we carried out a dose-finding experiment with MSC2363318A in an ovarian cancer model (Igrov1), and downstream markers were evaluated 12, 24, and 48 hours after the last dose. (Supplementary Figure 1A, available online). A reduction in expression of downstream p-ribosomal S6 protein and a resultant increase in $pAKT^{473}$ (from feedback loops) were observed at doses of 20 and 40 mg/kg, as previously reported (13). A maximum tolerated dose experiment was then performed in non-tumor-bearing mice after daily treatment for 14 consecutive days with MSC2363318A with or without paclitaxel. Body weight percentage differences were observed in all groups treated that included MSC2363318A, but weight loss was the least in the monotherapy and combination groups at the 25 mg/kg dose (Supplementary Figure 1B, available online). Therefore, daily administration of 25 mg/kg was chosen for subsequent

experiments. No deaths were observed in any treatment group, and weight was partially recovered during treatment.

Next, we carried out a series of experiments to characterize the therapeutic efficacy of MSC2363318A. In the SKOV3ip1 model, tumor growth was statistically significantly decreased in mice treated with MSC2363318A and MSC2363318A with paclitaxel compared with control (control: 1.9 g, SD = 2.0; MSC2363318A: 0.14 g, SD = 0.14, $P = .04$; MSC2363318A and paclitaxel: 0.12 g, SD = 0.12, $P = .03$) (Figure 1A). Less distant metastases were observed at necropsy in monotherapy and combination therapy groups (Figure 1, B and C), and reductions in tumor nodules were observed in all treatment groups (Supplementary Figure 1C, available online). There was a 16.8% to 17.6% decrease in mouse body weight, but no noticeable changes in mobility, feeding habits (Supplementary Figure 1D, available online), or deaths were noted during drug treatment. A reduction in downstream p-ribosomal S6 protein was seen in both groups treated with MSC2363318A (Supplementary Figure 1E, available online). In the Igrov1 model (Supplementary Figure 2, A to C, available online), similar results for tumor growth and metastatic spread were noted. Mice treated with MSC2363318A had decreased weight, and combination MSC2363318A and paclitaxel-treated mice had the fewest metastatic nodules (Supplementary Figure 2, D and E, available online).

We also examined the biological effects of MSC2363318A in orthotopic uterine cancer models. Ten days following inoculation of Hec1a cells into the uterine horn, treatment with MSC2363318A and paclitaxel was initiated. In the Hec1a model, tumor growth was statistically significantly decreased in mice treated with MSC2363318A with paclitaxel compared with control (control: 0.98 g, SD = 0.68; MSC2363318A and paclitaxel: 0.14 g, SD = 0.13, $P < .001$) (Figure 1D). The most statistically significant reduction in distant metastatic sites occurred with combination treatment (Figure 1, E and F; Supplementary Figure 2F, available online); there was modest reduction in mouse weights in the MSC2363318A treatment groups (Supplementary Figure 2G, available online). A reduction in downstream p-ribosomal S6 protein was seen in both groups treated with MSC2363318A (Supplementary Figure 2H, available online). Given the robust antitumor effects of MSC2363318A-based therapy, we investigated whether survival could be improved by such therapy in the SKUT2 model, which has both PTEN and PIK3CA mutations, leading to increased pathway activation. Survival was analyzed by the Kaplan-Meier method ($P < .001$). Mice treated with combination MSC2363318A and paclitaxel had the longest overall survival (mean = 104.2 days, 95% confidence interval [CI] = 97.0 to 111.4 days) compared with those treated with vehicle (mean = 61.9 days, 95% CI = 46.3 to 77.5 days), MSC2363318A alone (mean = 89.7 days, 95% CI = 83.0 to 96.4 days), and paclitaxel alone (mean = 73.6 days, 95% CI = 53.4 to 93.8 days) (Figure 1G). To evaluate the effect of MSC2363318A on tumor reduction, mice were injected with luciferase-labeled Ishikawa cells (PTEN mutant) and monitored with IVIS imaging (Figure 1H). Regression and stabilization of established tumors were observed in mice treated with combination MSC2363318A and paclitaxel (Figure 1I).

Biological Effects of MSC2363318A on Proliferation and Apoptosis

In the SKOV3ip1 model, treatment with combination MSC2363318A and paclitaxel resulted in the greatest reduction of cellular proliferation as determined by Ki67 (mean = 18.0 Ki67-positive cells per high-powered field [HPF], 95% CI = 5.2 to 30.8) compared with vehicle (mean = 105.9 positive cells per HPF, 95% CI = 99.7 to 112.1), MSC2363318A alone (mean = 89.9 positive cells per HPF, 95% CI = 76.9 to 102.9), and paclitaxel alone (mean = 51.4 positive cells per HPF, 95% CI = 45.3 to 57.5). Increased cleaved caspase 3–positive cells per HPF were observed after treatment with MSC2363318A alone (mean = 34.7 positive cells per HPF, 95% CI = 20.0 to 49.3) and combination MSC2363318A with paclitaxel (mean = 32.2 positive cells per HPF, 95% CI = 17.9 to 46.5) compared with vehicle (mean = 12.1 positive cells per HPF, 95% CI = 9.7 to 14.5) and paclitaxel (mean = 22.6 positive cells per HPF, 95% CI = 16.0 to 29.1) (Figure 2A). Statistically significant reductions in CD31 and Ki67 with increases in cleaved caspase 3 occurred in the combination MSC2363318A and paclitaxel-treated mice inoculated with Igrov1 cells (Supplementary Figure 3, available online). In the Hec1a model, all treatment groups had a statistically significant reduction in Ki67, but this effect was most pronounced in the combination MSC2363318A and paclitaxel group (mean = 90.0 Ki67-positive cells per HPF, 95% CI = 79.8 to 100.1). An increase in cleaved caspase 3 was observed in the Hec1A model after treatment with MSC2363318A alone (mean = 9.6 positive cells per HPF, 95% CI = 8.0 to 11.1) and MSC2363318A with paclitaxel (mean = 11.1 positive cells per HPF, 95% CI = 8.0 to 14.2).

In Vitro Effect of MSC2363318A in Ovarian and Uterine Cancer Cell Lines

The effect of MSC2363318A on a panel of 10 ovarian cancer cell lines was tested, and IC50 levels ranged from 0.7 to 12.9 μM (Figure 3A). Ovca432 was identified as the most sensitive (IC50 = 0.7 μM), and SKOV3ip1 was the most resistant (IC50 = 12.9 μM). In a panel of nine uterine cancer cell lines, the IC50 ranged from 0.0004 to 33.8 μM (Figure 3B). AN3CA and KLE were the most sensitive and resistant cell lines, respectively. Cell lines were characterized by mutation status, and we hypothesized that those mutations leading to activation of the PI3K/AKT pathway (such as PTEN-inactivating mutations and PIK3CA mutations) would be the most sensitive to MSC2363318A inhibition (Table 1).

Because of the inhibition of tumor growth and proliferation in vivo, we tested these effects in vitro using resistant (defined as IC50 $\geq$ 5 μM) ovarian and uterine cancer cell lines, SKOV3ip1 and Ishikawa, respectively. We observed decreased proliferation in both cell lines when treated daily at the previously calculated concentrations that inhibited 20% of cell growth (IC20) and IC50 doses (Figure 3C). This was also validated in sensitive (IC50 < 5 μM) ovarian and uterine cancer cell lines, Igrov1 and Hec1b, respectively, at both concentrations (Supplementary Figure 4A, available online). Next, we examined the molecular signaling events involved in the PI3K/AKT pathway after treatment with varying concentrations of MSC2363318A. The expression level of downstream targets, pPRAS-40, and p-ribosomal S6 protein were reduced after treatment of SKOV3ip1 at concentrations above 0.1 μM (Figure 3D) between one and 24 hours (Supplementary Figure 4B, available online).

Paclitaxel, in combination with MSC2363318A, contributed to the most profound in vivo effects and was tested in vitro. There was a dose-dependent decrease in cell viability after combination therapy with paclitaxel at the IC20 and IC50 concentrations of MSC2363118A. The combination index (CI), obtained after performing an isobologram analysis, showed synergistic cytotoxicity in Ishikawa and SKOV3ip1 cells with these two treatments (Figure 3, E and F). The only other cell line that showed

ARTICLE

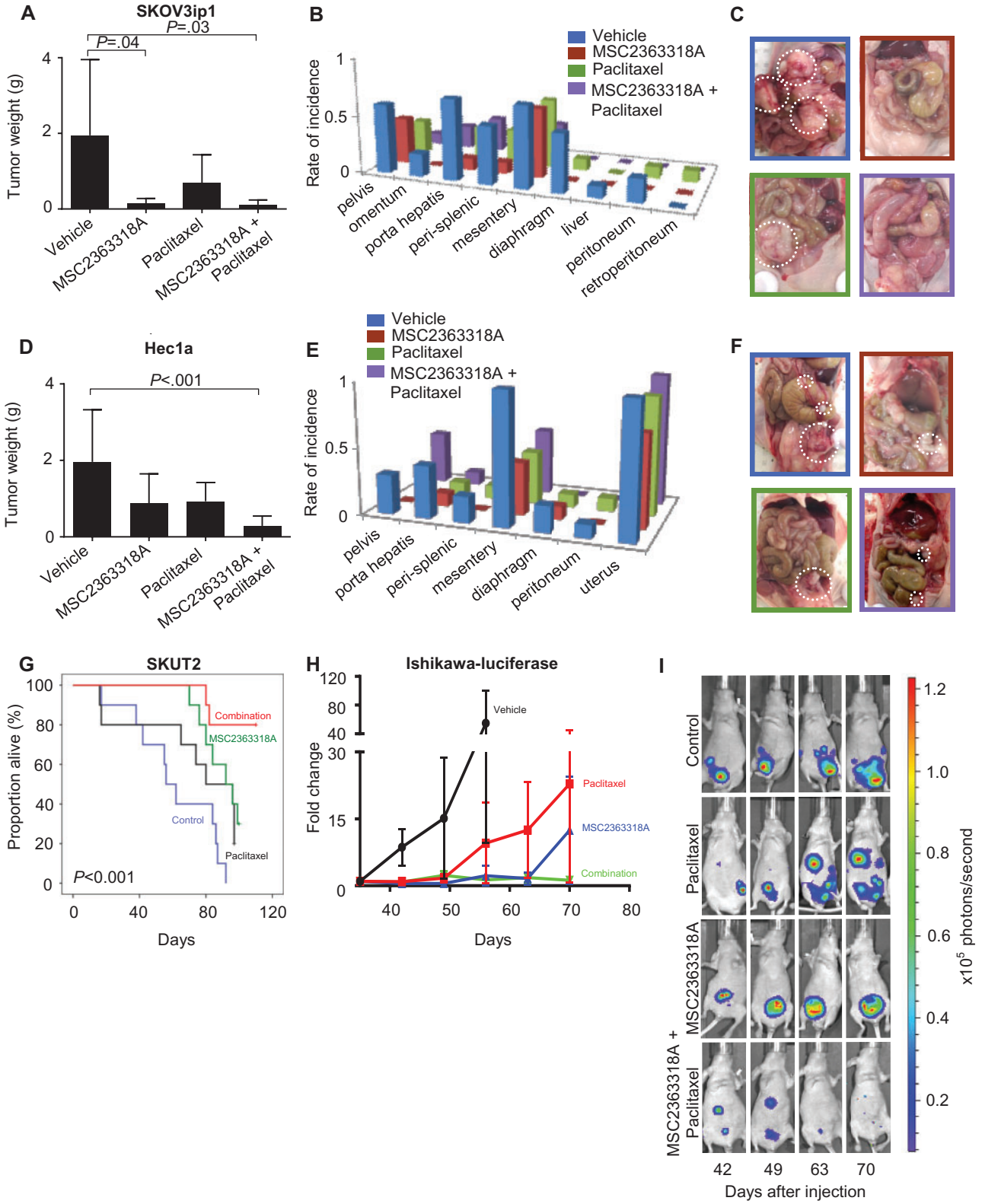

Figure 1. Effects of MSC2363318A on ovarian and uterine tumor growth. Mice inoculated with **(A–C)** SKOV3ip1 cells (intraperitoneally) and **(D–F)** Hec1a cells (via intrauterine injection) received vehicle (control), MSC2363318A (25 mg/kg oral daily), paclitaxel (4 mg/kg intraperitoneally weekly), or a combination of MSC2363318A and paclitaxel. Tumor growth and metastatic locations are shown (n = 10 per group). **G)** Survival of mice treated with vehicle (control), MSC2363318A, paclitaxel, or combination therapy in SKUT2 uterine orthotopic model (n = 10 per group). **H)** The effect of MSC2363318A on regression of established tumors from mice injected with Ishikawa-luciferase was evaluated. Mice were randomly assigned to treatment with vehicle, MSC2363318A, paclitaxel, or combination therapy. The same mouse from each group is shown at each time point (n = 7 per group). Photon measurements are from bioluminescence readings. Signal intensity was quantified as the sum of all detected photons within the region of interest per second (x10^5). **I)** Representative images from days 42, 49, 63, and 70 after cell injection are shown. **Error bars** represent the standard deviation (SD). Nonparametric Kruskal-Wallis test and Dunn's post-test for multiple comparisons. All statistical tests were two-sided.

ARTICLE

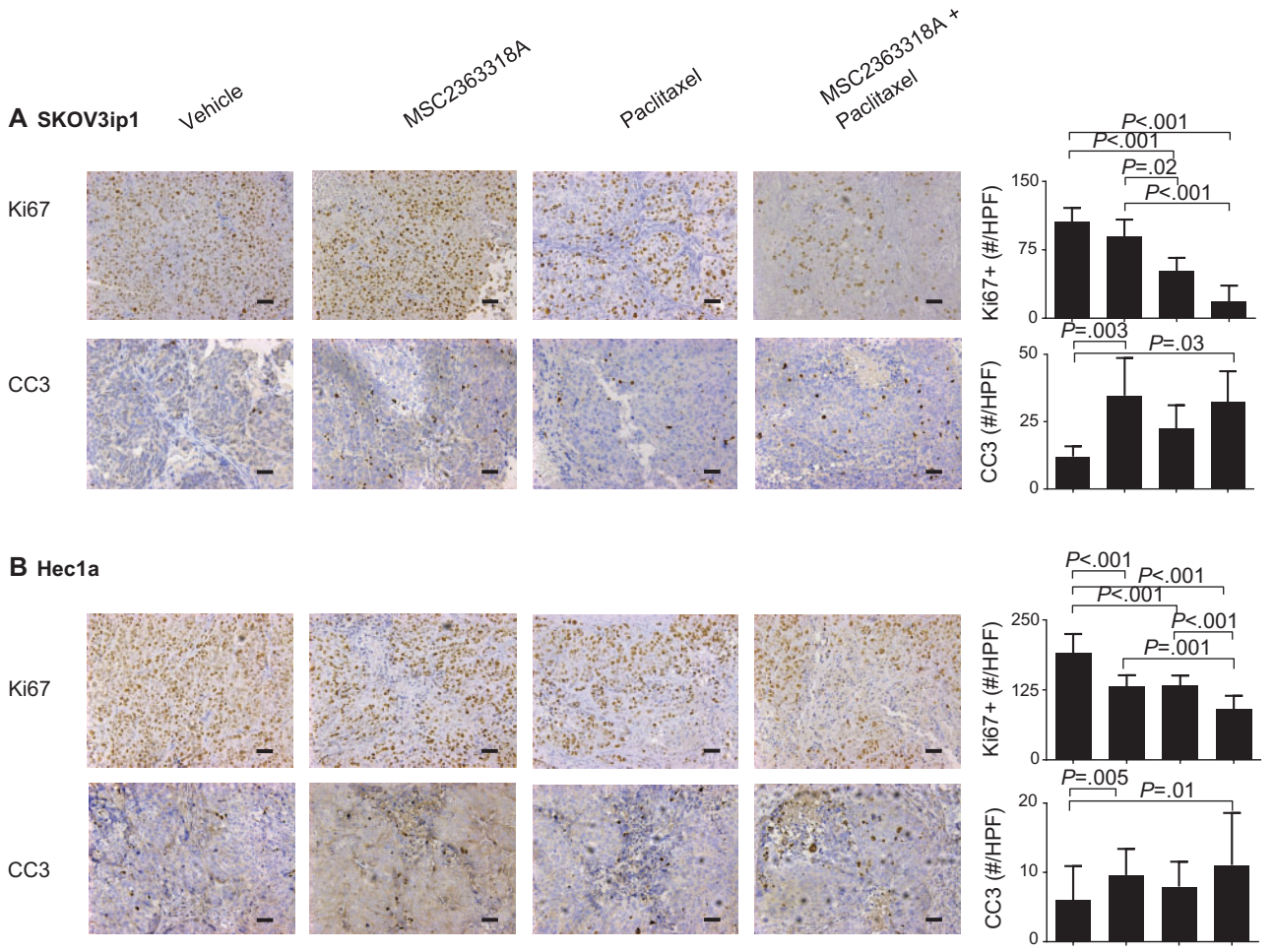

Figure 2. Effect of MSC2363318A on proliferation and apoptosis on ovarian and uterine tumors. **A)** SKOV3ip1 and **(B)** Hec1a tumors collected at the conclusion of in vivo therapeutic experiments, and immunohistochemical stains were performed to evaluate the effects of MSC23633318A, paclitaxel, or combination therapy on cancer cell proliferation (Ki67) and apoptosis (cleaved caspase 3 [CC3]) staining. Representative sections (final magnification, ×20) are shown for the four treatment groups. Each **scale bar** represents 100 μm. The mean Ki67-positive cells and mean cleaved caspase 3 cells are shown in the adjoining graphs. Five fields per slide and at least five slides per treatment group ($n \geq 25$) were examined. **Error bars** represent the SD. Nonparametric Kruskal-Wallis test and Dunn's post-test for multiple comparisons. All statistical tests were two-sided.

ARTICLE

similar synergy was SKUT2 (Supplementary Figure 4C, available online). In the Igrov1 and Hec1b cell lines, concurrent paclitaxel and MSC2363318A treatment at IC20 and IC50 doses demonstrated additive effects (Supplementary Figure 4, D and E, available online). Combination MSC2363318A with paclitaxel also contributed to a statistically significant increase in apoptosis rates in SKOV3ip1 and Ishikawa (Supplementary Figure 4F, available online).

YAP1 as a Predictor of In Vitro Response to MSC2363318A

To identify potential markers of response to MSC2363318A, we used RPPAs after treatment of ovarian (Igrov1 and Ovcar5) and uterine (Hec1b, Ishikawa, KLE, and RL95-2) cancer cell lines (Figure 4A). Network analysis identified the top networks that were activated in the ratio of resistant to sensitive cell lines (Table 2). Given the robust in vitro and in vivo effects on angiogenesis, we investigated the upregulated pro-angiogenic signaling molecules by a network overlaid with the ratio of resistant to sensitive total protein changes (Figure 4B). After further analysis of only resistant cell lines with and without MSC2363318A treatment, we observed an increase in total YAP1 levels (Supplementary Figure 5A, available online), which was not seen in the sensitive cell lines (Supplementary Figure 5B, available online). We plotted the logarithmic ratio values for YAP1 and pYAP1 from the cell lines using the RPPA data of the treated over untreated ratio (Figure 4C). There was higher total YAP1 expression in resistant cell lines, and we validated our findings by immunoblot analysis (Supplementary Figure 5C, available online). Mean YAP1 protein expression from the immunoblot replicates (Figure 4D) were evaluated and quantified in a panel of uterine and ovarian cancer cell lines, and a Spearman's correlation was performed ($R = 0.54$, $P = .02$), suggesting that more resistant cell lines have higher YAP1 expression and vice versa (Figure 4E).

To address the role of YAP1 overexpression and resistance to MSC2363318A, we transfected Ovca432, Igrov1, and Hec1b cells with YAP1 or empty vector and characterized them by

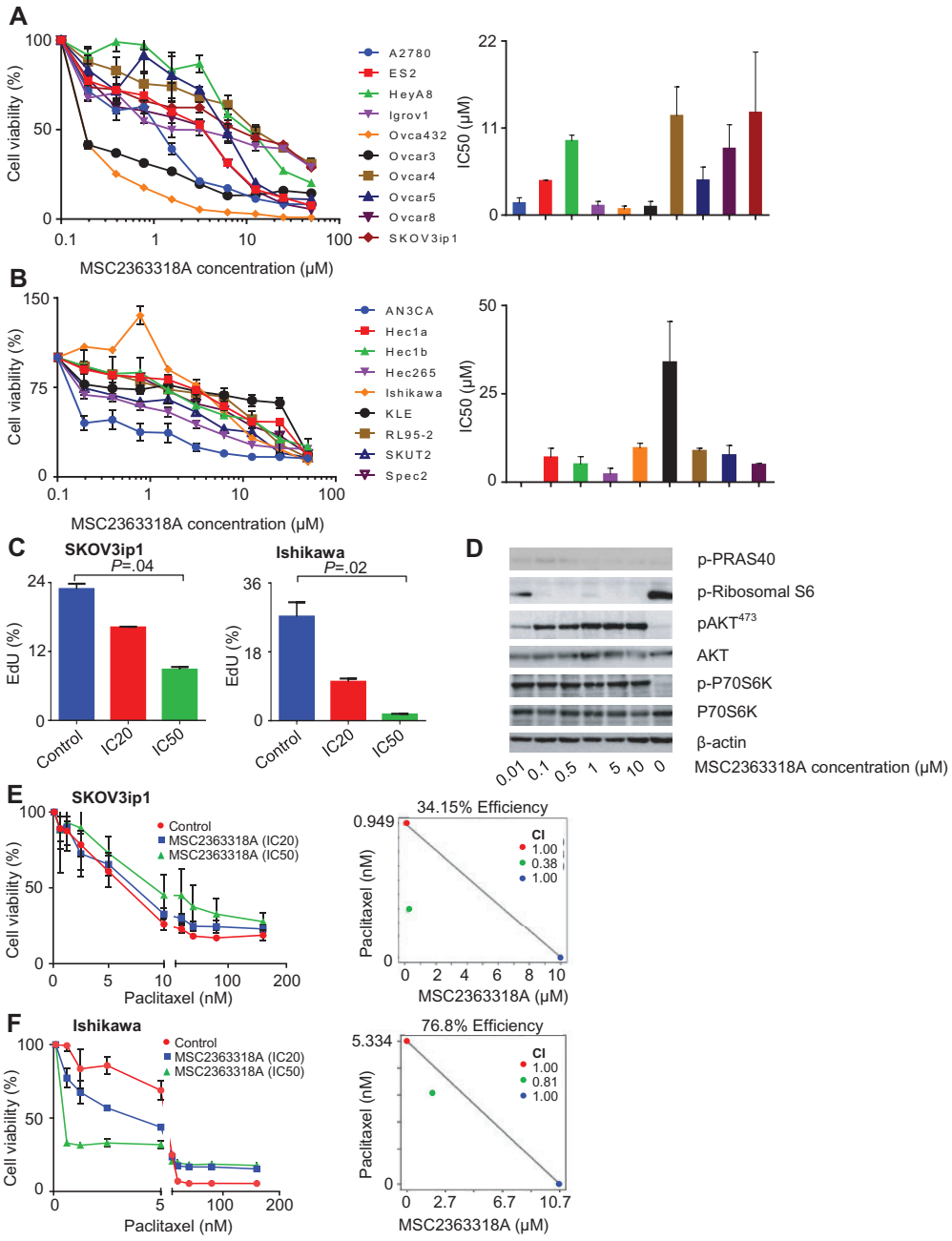

Figure 3. Effects of MSC2363318A on ovarian and uterine cancer cell lines. **A)** Cell viability after treatment with MSC2363318A between 0 to 50 μM for 96 hours and mean inhibitory concentration (IC50) after treatment with MSC2363318A in ovarian and **(B)** uterine cancer cell lines. Data represent average of triplicate measurements, and **error bars** represent the SD. **C)** Percentage of EdU incorporation in SKOV3ip1 and Ishikawa cells treated daily with control (PBS) and MSC2363318A at cell line–specific IC20 and IC50 concentrations measured after 72 hours. Data represent average of triplicate measurements, and **error bars** represent the SD. **D)** Immunoblot analyses of downstream and pathway markers after treatment of SKOV3ip1 cells with 0, 0.01, 0.1, 0.5, 1, 5, and 10 μM concentrations of MSC2363318A after 18 hours. **E)** SKOV3ip1 and **(F)** Ishikawa were treated with different concentrations of paclitaxel alone or in combination with the cell line–specific IC20 or IC50 for 96 hours followed by MTT analysis to determine percent cell viability. The combination index (CI) was calculated after performing isobologram analysis. A CI of less than 1.0 indicates synergism, a CI of 1 indicates additive activity, and a CI of more than 1.0 indicates antagonism. **Error bars** represent the SD. Nonparametric Kruskal-Wallis test and Dunn's post-test for multiple comparisons. All statistical tests were two-sided.

immunoblot (Supplementary Figure 5D, available online). There were minimal differences in cell viability after treatment with MSC2363318A in the cell lines with empty vector or YAP1 (Supplementary Figure 5E, available online). We did not observe increased pAKT^{473} expression in the YAP1-expressing cells after MSC2363318A treatment (Supplementary Figure 5F), suggesting that resistance to MSC2363318A is correlated with, but not dependent on, YAP1 overexpression. To further test our hypothesis, YAP1 gene expression was obtained from the publicly available NCI-60 CellMiner (14) for breast cancer cell lines with previously reported MSC2363318A IC50s (13) and for the ovarian cancer cell lines evaluated. A Spearman's correlation was performed ($R = 0.47$, $P = .13$) (Supplementary Figure 5G, available online).

ARTICLE

Table 1. Mutation status of ovarian and uterine cancer cell lines*

Cell line	AKT1	AKT2	AKT3	PIK3CA	RPS6KB2	PTEN
Uterine cancer cell lines						
AN3CA	WT	WT	WT	WT	WT	Mut p.R130fs
Hec1a	WT	WT	WT	Mut p.G1049R	WT	WT
Hec1b	WT	WT	WT	Mut p.G1049R	WT	WT
Hec265	WT	WT	WT	WT	WT	Mut p.L318fs
Ishikawa	WT	Mut p.Y273H	WT	WT	WT	Mut p.E288fs, p.V317fs
KLE	WT	WT	WT	WT	WT	WT
RL952	WT	WT	WT	WT	WT	Mut p.M134I, p.R173H
SKUT2	WT	WT	WT	Mut p.R88Q	WT	Mut p.T321fs, p.V317fs
Ovarian cancer cell lines						
A2780	WT	WT	WT	Mut p.E365K	WT	Mut p.KGR128del
ES2	WT	WT	WT	WT	WT	WT
HeyA8	WT	WT	WT	WT	Mut p.T366M	WT
Igrov1	WT	WT	WT	Mut p.R38C	WT	Mut p.V317fs, p.Y155C
OVCAR3	WT	WT	WT	WT	WT	WT
OVCAR4	WT	WT	WT	WT	WT	WT
OVCAR8	WT	WT	WT	WT	WT	WT
SKOV3ip1	WT	WT	WT	Mut p.H1047R	WT	WT

*Mut = mutant; WT = wild-type.

ARTICLE

Anti-angiogenic Effects of MSC2363318A and Bevacizumab

To address whether MSC2363318A affects endothelial cells in vitro, we assessed endothelial cell tube formation. A decrease in the number of nodes formed was observed after treatment of bevacizumab-sensitive RF-24 endothelial cells with MSC2363318A monotherapy (mean = 15.4 number of nodes per HPF, 95% CI = 9.2 to 14.0) and combination therapy (with bevacizumab; mean = 6.1 number of nodes per HPF, 95% CI = 3.8 to 8.4) compared with control (mean = 35.4 number of nodes per HPF, 95% CI = 30.0 to 40.8) (Figure 5A). Clinically, patients develop resistance to anti-angiogenic therapies, so we established a bevacizumab-resistant RF-24 clone (Supplementary Figure 6A, available online). Cell viability was assessed for the sensitive and resistant RF-24 cells (Supplementary Figure 6B, available online), and the sensitive line had a statistically significantly lower IC50 ($P < .001$). Endothelial cell tube formation was assessed in the resistant RF-24 cell line (Figure 5B). We observed a statistically significant reduction in percent EdU incorporation in both the sensitive and resistant RF-24 cell lines treated with combination MSC2363318A and bevacizumab (Supplementary Figure 6C, available online). The addition of MSC2363318A and bevacizumab to resistant RF-24 cells led to a 78.5% reduction in the MSC2363318A IC50, which was less than the MSC2363318A IC50 of sensitive RF-24 cells (Figure 5C). Treatment of resistant and sensitive RF24 cells with 1 μM of MSC2363318A led to a reduction of p-S6 ribosomal protein and increase in $pAKT^{473}$ (Supplementary Figure 6D, available online).

Next, we evaluated the effects of MSC2363318A on angiogenesis in vivo. In the SKOV3ip1 tumor model, there was decreased MVD after treatment with MSC2363318A alone (mean = 7.8 positive cells per HPF, 95% CI = 5.3 to 10.3) or in combination with paclitaxel (mean = 7.5 positive cells per HPF, 95% CI = 5.8 to 9.3) compared with control (mean = 20.4 positive cells per HPF, 95% CI = 13.9 to 27.0) (Figure 6A). Similar effects on CD31 were observed in the Hec1a orthotopic murine model (Figure 6B). We further investigated the effects of MSC2363318A in combination with bevacizumab. Substantial reductions in tumor weight were observed in all groups, but most profoundly (96.2% reduction compared with control) in the group treated with MSC2363318A and bevacizumab (Figure 6, C to E). Although mouse weight was decreased in the combination bevacizumab and MSC2363318 group compared with control, this was not statistically significant (Supplementary Figure 6E, available online). Tumor nodules were decreased in all treatment groups (Supplementary Figure 6F, available online). In the HeyA8 tumors, there was decreased MVD after treatment with MSC2363318A alone (mean = 6.6 positive cells per HPF, 95% CI = 4.9 to 8.3) and in combination with bevacizumab (mean = 6.3 positive cells per HPF, 95%

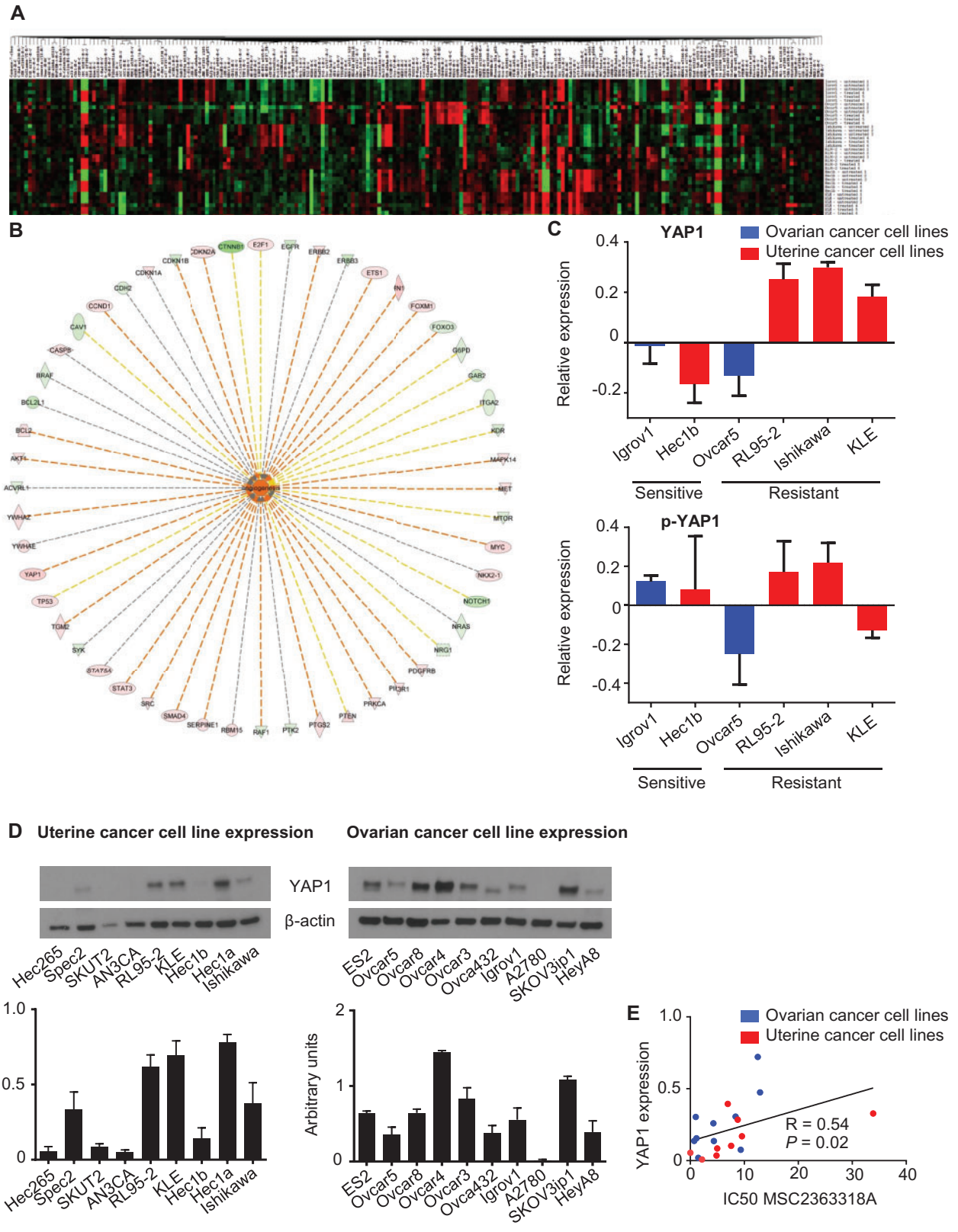

Figure 4. Differential expression of proteins in the PI3K/AKT/P70S6 signaling pathway after MSC2363318A treatment as detected by reverse-phase protein array. **A)** Heatmap of proteins whose expression was different before and after treatment with MSC2363318A (1 μM) for 18 hours. **B)** Upregulated pro-angiogenic signaling molecules by a network overlaid with the ratio of resistant to sensitive total protein change using ingenuity pathway analysis. **C)** Logarithmic ratio values for YAP1 and p-YAP1 in cancer cell lines. Protected cell lines were classified by an IC50 of 5 μM or greater. **D)** Expression of YAP1 in uterine and ovarian cancer cell lines and quantification of immunoblots. **Error bars** represent the SD. E) Spearman's correlation (R) of YAP1 protein expression and cell line–specific IC50 for MSC2363318A. All statistical tests were two-sided.

Table 2. Top 10 networks in the ratio of resistant to sensitive ovarian and uterine cancer cell lines

Diseases or functions annotation	P*	Predicted	Activation z-score	No. of molecules
Metabolism of DNA	2.45×10^{-33}	Increased	2.657	44
Apoptosis of tumor cell lines	2.61×10^{-71}	Increased	2.311	102
Degradation of DNA	8.50×10^{-24}	Increased	2.240	27
Apoptosis of bone cancer cell lines	4.88×10^{-24}	Increased	2.238	24
Leukocyte migration	4.76×10^{-25}	Increased	2.204	52
Angiogenesis	2.15×10^{-29}	Increased	2.132	52
Apoptosis of tumor cells	1.40×10^{-40}	Increased	2.060	44
Apoptosis of leukemia cell lines	3.91×10^{-37}	Increased	2.043	41
Cell death of tumor cells	5.34×10^{-40}	–	2.000	48
Necrosis of tumor	9.72×10^{-41}	–	2.000	49

*A right tail Fisher exact test was used to calculate the *P* values. No prediction could be made when the Activation z score is equal to 2.000.

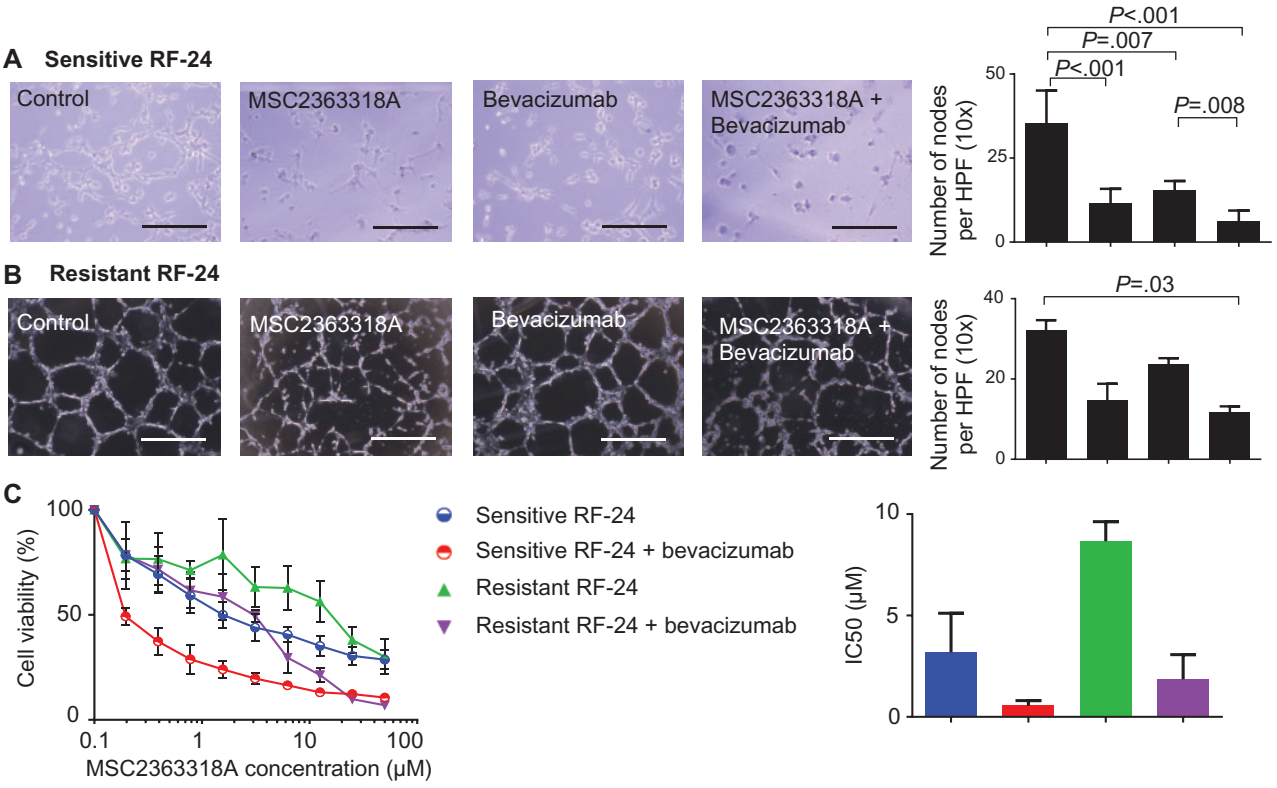

Figure 5. In vitro effects of MSC2363318A in combination with anti-angiogenic therapy. **A and B)** Representative pictures of endothelial vessel formation of sensitive and bevacizumab-resistant RF-24 cells and quantification of the number of nodes (points at which where three or more elongated cells meet) formed on the gel matrix after prior treatment with 0.5 mg of bevacizumab, the cell line–specific IC20 of MSC2363318A, or combination therapy; n = 3 wells per group and mean number of nodes is quantified from five pictures per well. Images were taken at 40× magnification. Each **scale bar** represents 100 μm. **C)** Viability of sensitive and bevacizumab-resistant RF-24 cells after treatment with MSC2363318A between 0 to 50 μM ± 0.5 mg of bevacizumab for 96 hours and mean inhibitory concentration (IC50). Data represent average of triplicate measurements, and **error bars** represent the SD. Nonparametric Kruskal-Wallis test and Dunn's post-test for multiple comparisons. All statistical tests were two-sided.

CI = 4.6 to 8.0) compared with vehicle (mean = 15.4 positive cells per HPF, 95% CI = 10.6 to 20.3) (Figure 6F). Treatment with MSC2363318A and bevacizumab resulted in decreased cellular proliferation and increased apoptosis (Supplementary Figure 6G, available online).

Because of the emergence of resistance to anti-angiogenesis therapy clinically, we investigated the efficacy of MSC2363318A in models of adaptive resistance. After intraperitoneal establishment of luciferase-labeled SKOV3ip1 ovarian tumors, mice were randomly assigned to two treatment groups: 1) control and 2) bevacizumab treatment. Mice receiving bevacizumab treatment were subsequently divided into bevacizumab-sensitive or -resistant groups based on imaging. Bevacizumab-resistant mice were defined as those with increased tumor growth as evidenced by increased bioluminescence intensity in previously stable tumor burden (Figure 6G). At the emergence of resistance, MSC2363318A was added to bevacizumab treatment. The addition of MSC2363318A at the emergence of resistance

ARTICLE

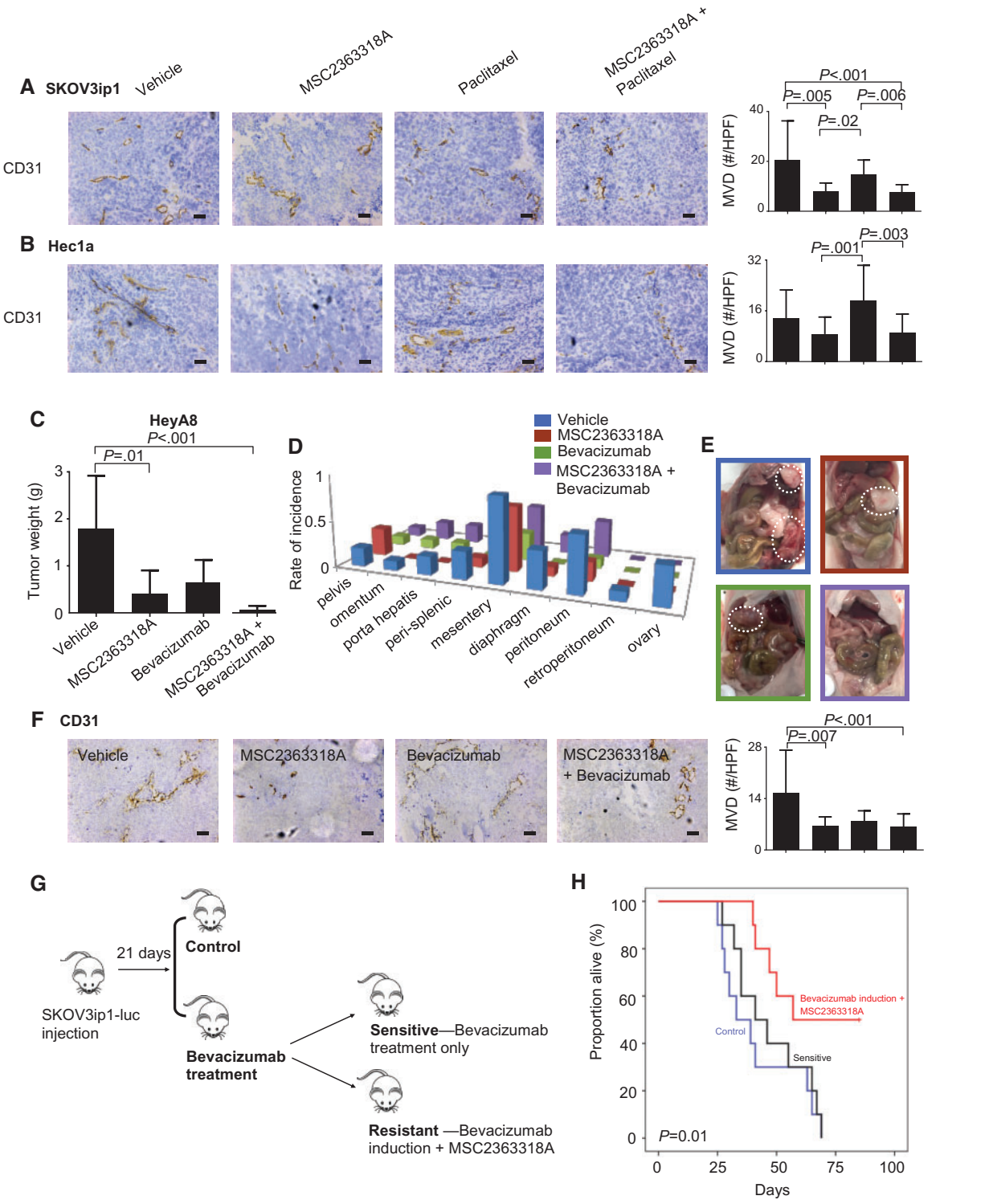

Figure 6. In vivo effects of MSC2363318A in combination with anti-angiogenic therapy. Immunohistochemistry was performed to evaluate the effects of MSC23633318A, paclitaxel, or combination therapy on tumor-associated angiogenesis (CD31). Representative sections (final magnification, ×20) are shown for the four treatment groups with the average number of CD31-positive vessels per field in mice inoculated with SKOV3ip1 **(A)** and Hec1a **(B)**. Each **scale bar** represents 100 μm. Mice inoculated with HeyA8 ovarian cancer cells **(C–E)** received vehicle (control), MSC2363318A (25 mg/kg oral daily), bevacizumab (6.25 mg/kg intraperitoneally twice weekly), or a combination of MSC2363318A and bevacizumab beginning 10 days after inoculation. Tumor size and sites of metastases were recorded, and representative pictures are shown (n = 10 mice per group). **F)** Immunohistochemistry was performed to evaluate the effects of MSC23633318A, bevacizumab, or combination therapy on cancer cell angiogenesis as determined by CD31 quantification. Representative sections (final magnification, ×20) are shown for the four treatment groups with the average number of CD31-positive vessels per field in mice. **G)** Schematic for experiment when mice were injected with luciferase-labeled SKOV3ip1 cells and bioluminescence imaging was used to confirm tumor. After 21 days, mice received vehicle (control) or bevacizumab (6.25 mg/kg twice weekly). Mice were subsequently divided into groups depending on the sensitivity of their tumor to anti-angiogenic therapy. The resistant group received MSC2363318A. **H)** Survival of these groups is shown (n = 10 in control and resistant groups; n = 14 in sensitive group). **Error bars** represent the SD. Nonparametric Kruskal-Wallis test and Dunn's post-test for multiple comparisons. All statistical tests were two-sided.

ARTICLE

halted tumor growth and prolonged survival, as compared with either control or bevacizumab treatment alone using the Kaplan-Meier method ($P = .01$) (Figure 6H). Mice treated with bevacizumab induction followed by MSC2363318A had the longest overall survival (mean = 66.0 days, 95% CI = 53.9 to 78.1) compared with mice treated with vehicle (mean = 42.0 days, 95% CI = 31.4 to 52.6) and bevacizumab-sensitive mice (mean = 47.2 days, 95% CI = 37.5 to 56.9).

Discussion

The key findings in this manuscript are that dual inhibition of AKT and P70S6K has therapeutic efficacy in multiple preclinical models by enhancing cellular apoptosis, inhibiting proliferation, and reducing angiogenesis. Synergy was observed in both ovarian and uterine cancer cell types with the combination of MSC2363318A and paclitaxel. Addition of MSC2363318A to antiangiogenic therapy potentiated the effects of bevacizumab and restored sensitivity in the adaptive resistance setting. Finally, we identified YAP1 as marker that correlates with sensitivity to inhibition with MSC2363318A.

Genetic and/or epigenetic changes lead to activation of the PI3K/AKT signaling pathway in multiple cancers. Additionally, previous analyses have found this pathway to be activated in half of high-grade serous ovarian carcinomas. Uterine cancers harbor the highest rates of PI3K/AKT pathway alterations, including PTEN mutations (15,16). Other frequently identified pathway mutations in uterine cancer include PIK3CA (25%–40%), PIK3R1 (15%–25%), and less commonly, AKT1-3 mutations (2%–5%) (17–20). PI3K/AKT activation in gynecologic malignancies provides the rationale for development and testing of therapies targeting this signaling pathway.

The first PI3K inhibitors (eg, Wortmannin and LY294002) led to pan-inhibition of this pathway, but their therapeutic potential remained limited (21). Second-generation PI3K inhibitors targeted specific PI3K isoforms and are being evaluated in preclinical and clinical studies. The third generation inhibitors include dual PI3K/mTOR inhibitors, which targeted PI3K class I isoforms and mTOR complexes 1 and 2 and lead to greater inhibition of the entire pathway (22). Three isoforms of AKT possess biologic relevance in cancer pathogenesis, and phosphorylation activates multiple downstream signaling cascades including tuberous sclerosis complex 2 (TSC2) protein, tuberous sclerosis 1 (TSC1), mTOR, BAD, and caspase-9 (22,23). AKT inhibitors in preclinical and clinical development include perifosine, MK-2206, RX-0201, Erucylphosphocholine, PBI-05204, GSK690693, and XL-418 (23,24). XL-418, which inhibited both AKT and P70S6K, was tested in a phase I clinical trial in patients with advanced solid tumors. This study ended because of low drug exposure (NCT00460278). Previous mTOR complex-1 (mTORC1) inhibitors including everolimus or temsirolimus have been efficacious clinically, but their activity may be limited to the AKT pathway feedback loop activation (25,26). This is via induction of insulin receptor substrate-1 expression and abrogation of feedback inhibition within the PI3K/AKT pathway, which may cause hypersensitivity to inhibitors of the PI3K/AKT pathway. Inhibition of P70S6K further downstream confers a potential advantage over previously developed PI3K/AKT pathway inhibitors and can overcome activation of AKT in the feedback loop. Consistent with previous reports, MSC2363318A-treated cells have increased $pAKT^{473}$ expression, suggesting activation of the phosphorylated substrate, but pPRAS40 was not increased compared with control cells, which suggests successful inhibition of AKT activity. Historical studies have also shown a reduction in pGSK3α/β, providing further evidence of AKT inhibition (13).

Yes-associated protein (YAP) is one of the main downstream effectors of the Hippo signaling pathway, known to play a role in many oncogenic features (27,28). Unphosphorylated YAP translocates and accumulates in the nucleus, where it forms complexes with other transcriptional factors, leading to expression of target genes. Phosphorylated YAP promotes its cytoplasmic translocation and degradation. Previous studies have shown that levels and nuclear localization of YAP are elevated in some solid malignancies (29), including ovarian and endometrial cancer (30,31). Downregulation of the Hippo signaling pathway has been shown to promote ovarian cancer growth and is a key tumor suppressor pathway, but also makes ovarian cancer cells resistant to chemotherapy (28), specifically cisplatin (32). YAP1 signatures have been identified to be predictors of poor prognosis and survival (32–34), as well as those that may benefit from taxane-based chemotherapy (33). The PI3K/AKT pathway is hypothesized to interact in YAP-mediated drug resistance, and it has been previously shown that YAP is involved in crosstalk between the PI3K/AKT and Hippo signaling pathways (35,36). One possible mechanism for the elevated YAP1 expression could be via YAP1-mediated IGF expression and consequent activation of the PI3K/AKT pathway (37). Patients with ovarian and endometrial tumors with high YAP1 expression and increased PI3K/AKT activation could theoretically benefit the most from MSC2363318A.

The first phase I trial of MSC2363318A in patients with advanced malignancies has recently opened (NCT01971515). Future directions include administration of MSC2363318A as an adjuvant therapy in combination with taxane-based therapy after surgical cytoreduction. Moreover, MSC2363318A monotherapy could be tested in a maintenance therapy setting. Other alternatives include combining MSC2363318A with bevacizumab in patients with adaptive resistance. Finally, the identification of high YAP1 expression identifies those tumors that are most sensitive to inhibition by MSC2363318A. By identifying the subset of patients whose tumors would be most sensitive to dual AKT/P70S6K inhibition, lower treatment doses could be considered, overtreatment of patients who would not benefit could be avoided, and untoward toxicities in patients who will not respond could be prevented.

Our study has some potential limitations. Despite the safety of MSC2363318A in preclinical experiments, unexpected toxicities may be identified in early clinical trials. Further preclinical safety will need to be evaluated prior to future clinical development. In summary, MSC2363318A-based therapy may be therapeutically beneficial to ovarian and uterine cancer patients and YAP1 represents a potential predictive biomarker for sensitivity to this treatment.

Funding

This work was supported in part by National Institutes of Health (NIH) grants (P50CA083639, CA109298, P50CA098258, UH2TR000943, CA016672, U54CA96300, and U54CA96297), CPRIT (RP110595 and RP120214), an Ovarian Cancer Research Fund Program Project Development Grant, the Frank McGraw Memorial Chair in Cancer Research, the RGK Foundation, the Gilder Foundation, the Judi A. Rees Ovarian Cancer Research Fund, the Meyer and Ida Gordon Foundation, and the American Cancer Society Research Professor Award to AKS, Cancer Research UK to ALH, and the Ann Rife Cox Chair in Gynecology to RLC. This research was also supported in part by the Blanton-Davis Ovarian

ARTICLE

Cancer Research Program. GNAP was partially supported by the Science and Technology Grant from the Puerto Rico Science, Technology and Research Trust, Institutional Research Grant 14-189-19 from the American Cancer Society, and grants NIH P20GM103475, U54CA163071, U54CA163068 and G12MD007579. MH is supported by a fellowship of the Deutsche Forschungsgemeinschaft (DFG). RAP, HJD, and JMH are supported by NIH T32 Training Grant CA101642.

Notes

The study funders had no role in the design of the study; the collection, analysis, or interpretation of the data; the writing of the manuscript; or the decision to submit the manuscript for publication.

The authors declare that there are no conflicts of interest.

Authors: Rebecca A. Previs, Guillermo N. Armaiz-Pena, Cristina Ivan, Heather J. Dalton, Rajesha Rupaimoole, Jean M. Hansen, Yasmin Lyons, Jie Huang, Monika Haemmerle, Michael J. Wagner, Kshipra M. Gharpure, Archana S. Nagaraja, Justyna Filant, Michael H. McGuire, Kyunghee Noh, Piotr L. Dorniak, Sarah L. Linesch, Lingegowda S. Mangala, Sunila Pradeep, Sherry Y. Wu, Robert L. Coleman, Anil K. Sood.

Affiliations of authors: Department of Gynecologic Oncology and Reproductive Medicine (RAP, HJD, RR, JMH, YL, JH, MH, MJW, KMG, ASN, JF, MHM, KN, PLD, SLL, LSM, SP, SYW, RLC, AKS), Department of Cancer Biology (AKS), and Center for RNA Interference and Non-Coding RNAs (CI, LSM, AKS), The University of Texas MD Anderson Cancer Center, Houston, TX; Department of Basic Sciences, Division of Pharmacology, Ponce Health Sciences University, Ponce, Puerto Rico (GNAP); Division of Cancer Biology, Ponce Research Institute, Ponce, Puerto Rico (GNAP).

References

1. Hanahan D, Weinberg RA. Hallmarks of cancer: The next generation. *Cell*. 2011;144(5):646–674.
2. Samuels Y, Ericson K. Oncogenic PI3K and its role in cancer. *Curr Opin Oncol*. 2006;18(1):77–82.
3. Song MS, Salmena L, Pandolfi PP. The functions and regulation of the PTEN tumour suppressor. *Nat Rev Mol Cell Biol*. 2012:13:283–296.
4. Cancer Genome Atlas Research N. Integrated genomic analyses of ovarian carcinoma. *Nature*. 2011;474:609–615.
5. Obata K, Morland SJ, Watson RH, et al. Frequent PTEN/MMAC mutations in endometrioid but not serous or mucinous epithelial ovarian tumors. *Cancer Res*. 1998;58(10):2095–2097.
6. Yang HJ, Liu VW, Wang Y, Tsang PC, Ngan HY. Differential DNA methylation profiles in gynecological cancers and correlation with clinico-pathological data. *BMC Cancer*. 2006;6:212.
7. Gewinner C, Wang ZC, Richardson A, et al. Evidence that inositol polyphosphate 4-phosphatase type II is a tumor suppressor that inhibits PI3K signaling. *Cancer Cell*. 2009;16:115–125.
8. Carpten JD, Faber AL, Horn C, et al. A transforming mutation in the pleckstrin homology domain of AKT1 in cancer. *Nature*. 2007;448:439–444.
9. Cheng JQ, Godwin AK, Bellacosa A, et al. AKT2, a putative oncogene encoding a member of a subfamily of protein-serine/threonine kinases, is amplified in human ovarian carcinomas. *Proc Natl Acad Sci U S A*. 1992;89:9267–9271.
10. Levine DA, Bogomolniy F, Yee CJ, et al. Frequent mutation of the PIK3CA gene in ovarian and breast cancers. *Clin Cancer Res*. 2005;11:2875–2878.
11. Philp AJ, Campbell IG, Leet C, et al. The phosphatidylinositol 3'-kinase p85alpha gene is an oncogene in human ovarian and colon tumors. *Cancer Res*. 2001;61:7426–7429.
12. Kurman RJ, Shih Ie M. Molecular pathogenesis and extraovarian origin of epithelial ovarian cancer—shifting the paradigm. *Hum Pathol*. 2011;42:918–931.
13. Machl A, Wilker EW, Tian H, et al. M2698 is a potent dual-inhibitor of p70S6K and Akt that affects tumor growth in mouse models of cancer and crosses the blood-brain barrier. *Am J Cancer Res*. 2016;6:806–818.
14. NCI-60 CellMiner. https://discover.nci.nih.gov/cellminer/analysis.do. Accessed August 15, 2016.
15. Cancer Genome Atlas Research N, Kandoth C, Schultz N, et al. Integrated genomic characterization of endometrial carcinoma. *Nature*. 2013;497:67–73.
16. Whitman M, Downes CP, Keeler M, Keller T, Cantley L. Type I phosphatidylinositol kinase makes a novel inositol phospholipid, phosphatidylinositol-3-phosphate. *Nature*. 1988;332:644–646.
17. Urick ME, Rudd ML, Godwin AK, et al. PIK3R1 (p85alpha) is somatically mutated at high frequency in primary endometrial cancer. *Cancer Res*. 2011;71:4061–4067.
18. Rudd ML, Price JC, Fogoros S, et al. A unique spectrum of somatic PIK3CA (p110alpha) mutations within primary endometrial carcinomas. *Clin Cancer Res*. 2011;17:1331–1340.
19. Weigelt B, Banerjee S. Molecular targets and targeted therapeutics in endometrial cancer. *Curr Opin Oncol*. 2012;24:554–563.
20. Myers AP. New strategies in endometrial cancer: Targeting the PI3K/mTOR pathway—the devil is in the details. *Clin Cancer Res*. 2013;19:5264–5274.
21. Laplante M, Sabatini DM. mTOR signaling in growth control and disease. *Cell*. 2012;149:274–293.
22. Fruman DA, Rommel C. PI3K and cancer: Lessons, challenges and opportunities. *Nat Rev Drug Discov*. 2014;13:140–156.
23. Pal SK, Reckamp K, Yu H, Figlin RA. Akt inhibitors in clinical development for the treatment of cancer. *Expert Opin Investig Drugs*. 2010;19:1355–1366.
24. O'Reilly KE, Rojo F, She QB, et al. mTOR inhibition induces upstream receptor tyrosine kinase signaling and activates Akt. *Cancer Res*. 2006;66:1500–1508.
25. Wheler JJ, Moulder SL, Naing A, et al. Anastrozole and everolimus in advanced gynecologic and breast malignancies: Activity and molecular alterations in the PI3K/AKT/mTOR pathway. *Oncotarget*. 2014;5:3029–3038.
26. Emons G, Kurzeder C, Schmalfeldt B, et al. Temsirolimus in women with platinum-refractory/resistant ovarian cancer or advanced/recurrent endometrial carcinoma. A phase II study of the AGO-study group (AGO-GYN8). *Gynecol Oncol*. 2016;140:450–456.
27. Zanconato F, Cordenonsi M, Piccolo S. YAP/TAZ at the Roots of Cancer. *Cancer Cell*. 2016;29:783–803.
28. Guo L, Teng L. YAP/TAZ for cancer therapy: Opportunities and challenges (review). *Int J Oncol*. 2015;46:1444–1452.
29. Harvey KF, Zhang X, Thomas DM. The Hippo pathway and human cancer. *Nat Rev Cancer*. 2013;13:246–257.
30. Zhang X, George J, Deb S, et al. The Hippo pathway transcriptional co-activator, YAP, is an ovarian cancer oncogene. *Oncogene*. 2011;30:2810–2822.
31. Tsujiura M, Mazack V, Sudol M, et al. Yes-associated protein (YAP) modulates oncogenic features and radiation sensitivity in endometrial cancer. *PLoS One*. 2014;9:e100974.
32. Xia Y, Chang T, Wang Y, et al. YAP promotes ovarian cancer cell tumorigenesis and is indicative of a poor prognosis for ovarian cancer patients. *PLoS One*. 2014;9:e91770.
33. Jeong W, Kim SB, Sohn BH, et al. Activation of YAP1 is associated with poor prognosis and response to taxanes in ovarian cancer. *Anticancer Res*. 2014;34:811–817.
34. Xia Y, Zhang YL, Yu C, Chang T, Fan HY. YAP/TEAD co-activator regulated pluripotency and chemoresistance in ovarian cancer initiated cells. *PLoS One*. 2014;9:e109575.
35. Cai H, Xu Y. The role of LPA and YAP signaling in long-term migration of human ovarian cancer cells. *Cell Commun Signal*. 2013;11:31.
36. Qin LF, Ng IO. Induction of apoptosis by cisplatin and its effect on cell cycle-related proteins and cell cycle changes in hepatoma cells. *Cancer Lett*. 2002;175:27–38.
37. Fernandez LA, Squatrito M, Northcott P, et al. Oncogenic YAP promotes radioresistance and genomic instability in medulloblastoma through IGF2-mediated Akt activation. *Oncogene*. 2012;31:1923–1937.
38. Liu T, Hu W, Dalton HJ, et al. Targeting SRC and tubulin in mucinous ovarian carcinoma. *Clin Cancer Res*. 2013;19:6532–6543.
39. Chou TC. Drug combination studies and their synergy quantification using the Chou-Talalay method. *Cancer Res*. 2010;70:440–446.
40. Kang Y, Hu W, Ivan C, et al. Role of focal adhesion kinase in regulating YB-1-mediated paclitaxel resistance in ovarian cancer. *J Natl Cancer Inst*. 2013;105:1485–1495.